ORGANOMETALLICS

Article

Cite This: *Organometallics* 2019, 38, 1292−1299

pubs.acs.org/Organometallics

Manganese-Based Catalysts with Varying Ligand Substituents for the Electrochemical Reduction of CO_2 to CO

Steven E. Tignor, Hsin-Ya Kuo, Tia S. Lee, Gregory D. Scholes, and Andrew B. Bocarsly*

Department of Chemistry, Princeton University, Princeton, New Jersey 08544, United States

Supporting Information

ABSTRACT: A series of manganese complexes were synthesized with a variety of ligands and ligand substituents. These complexes were then studied using ultraviolet−visible spectroscopy, cyclic voltammetry, density functional theory calculations, and bulk electrolysis. The UV−vis, cyclic voltammetry, and calculation data show that the bipyridine π^* level is modulated by the incorporation of different substituents on the bipyridine and through this interaction moderates the observed catalytic activity of the complex toward CO_2 reduction. The calculations were correlated to the experimental UV−vis data and cyclic voltammetry data to demonstrate the relationship among these data, and a Hammett plot showed a good correlation between the substituent identity and the MLCT wavelength from UV−vis (R^2 = 0.96). When aliphatic substituents were placed on the 4,4′-positions of the bipyridine, the location of the bpy π^* was not significantly altered. However, when more electron withdrawing substituents were placed on the 4,4′-positions the bpy π^* level was altered more significantly. This alteration in the bpy π^* level had a profound effect on the rate of CO production determined from bulk electrolysis. While complexes whose bpy π^* level were similar or more blue shifted in comparison to the parent manganese complex did not display significantly altered efficiencies or rates for the conversion of CO_2 to CO, those species whose bpy π^* energies were significantly red shifted in comparison to the parent manganese complex displayed far poorer catalysis. This is postulated to be a combination of two factors. First, the singly reduced complex's ability to lose the axial bromide ligand is diminished when electron-withdrawing groups are placed on the bpy ligand due to an increasing gap between the bpy π^* and the Mn−Br σ^*. Second, the decreased electron density of the HOMO of the doubly reduced complex with electron-withdrawing groups makes the binding of a molecule of CO_2 less energetically favorable.

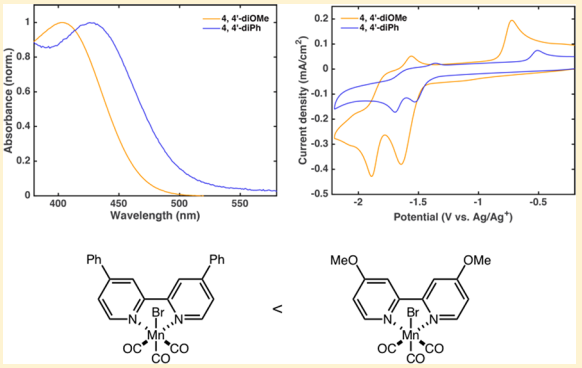

INTRODUCTION

The use of fossil fuels as an energy source continues to increase the global levels of carbon dioxide (CO_2) in our environment.[1,2] This continuing emission of CO_2 has highlighted the importance of determining ways in which CO_2 can be removed from the environment and utilized.[3,4] One attractive way to accomplish this is the electrochemical reduction of CO_2, which has been studied extensively through the use of metal electrodes[5−10] and surface-modified electrodes,[11−15] as well as soluble transition-metal catalysts.[16−22] Reduction of CO_2 to CO is attractive, since this provides a route to renewable syngas generation.[23]

This study is focused on a series of manganese-based soluble transition-metal complexes as catalysts for CO_2 reduction. These catalysts contain low-valent metal centers and are of the type *fac*-[MnX(N-N)(CO)$_3$], where X = halogen (or pseudohalogen) and N-N = a bipyridine (bpy) ligand, either modified or unmodified.[24−27] These catalysts are interesting from the perspective of precise tunability in addition to having high Faradaic efficiency for carbon monoxide production over the competing hydrogen evolution reaction (HER). Indeed, there have been several reports of modification to the ligand framework with the objectives of gaining insight into the mechanism by which these catalysts operate and increasing the rate or efficiency of CO production.[28−31] While there has been a substituent effect study done on the rhenium analogue by Clark et al.,[32] there are differences between the Mn and Re systems,[33] and to date there has not been a systematic study of the modification of the bipyridine ligand in these manganese systems to determine the effects on catalysis from such substitutions.

It has been shown that alteration of the ligand framework can modulate the catalysis of these prototypical manganese complexes.[34,35] From a detailed understanding of the mechanism of the reduction of CO_2 on these catalysts, it can be seen that these ligand alterations may have a significant effect on several steps in the catalytic cycle. It is generally agreed that this catalytic cycle begins with an initial one-electron reduction into the bipyridine π^* orbital (Figure 1).[36]

Special Issue: Organometallic Electrochemistry: Redox Catalysis Going the Smart Way

Received: August 2, 2018
Published: October 9, 2018

DOI: 10.1021/acs.organomet.8b00554
Organometallics 2019, 38, 1292−1299

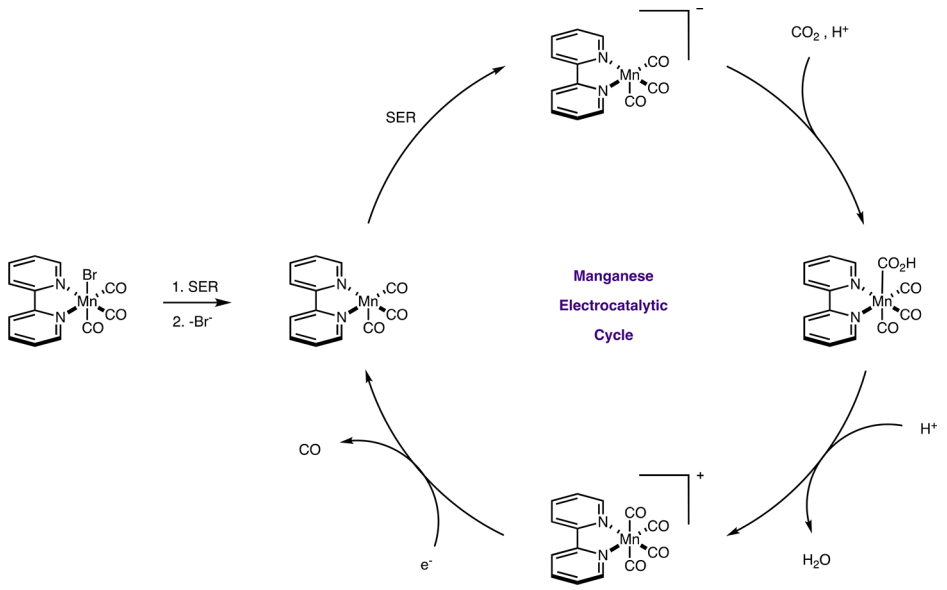

Figure 1. Catalytic cycle for $[Mn(bpy)(CO)_3Br]$-catalyzed CO_2 reduction. SER = single-electron reduction.

This reduction induces the dissociation of the axial halogen (or pseudohalogen) ligand, which opens up an axial coordination site. A second, one-electron reduction of this species produces an anionic manganese complex to which a molecule of CO_2 is able to add. Further reduction and protonation steps complete the catalytic cycle by regenerating the active manganese species and produce a molecule of CO.

We synthesized a variety of *fac*-$[MnX\text{-}(N\text{-}N)(CO)_3]$, complexes having a range of bipyridine substitutions as well as the complexes having 1,10-phenanthroline, bipyridine, or bipyrazine as the N-N ligand to study the effects varying substitution on the bipyridine. It is noted that it has already been shown that incorporation of bulky ligands on the bipyridine has impeded a nonproductive off-cycle dimerization step, and in addition a study on a variety of substituents has been conducted using the rhenium analogue of this system. It has also been reported that incorporating a proton donor substituent at the 6-position of the bipyridine ring introduces a hydrogen-bonding interaction that facilitates the kinetics of the catalytic cycle.[30,31] Additionally, important recent work has utilized a pendant Lewis base approach as a way to shift the catalysis toward a protonation-first pathway as opposed to a reduction-first pathway invoked at higher overpotentials.[37] The uses of both pendant hydrogen bond donors and pendant Lewis basic groups have proven to be fruitful ways to augment these catalysts. However, beyond these specific interactions, general substituent trends for the Mn system have not been analyzed.

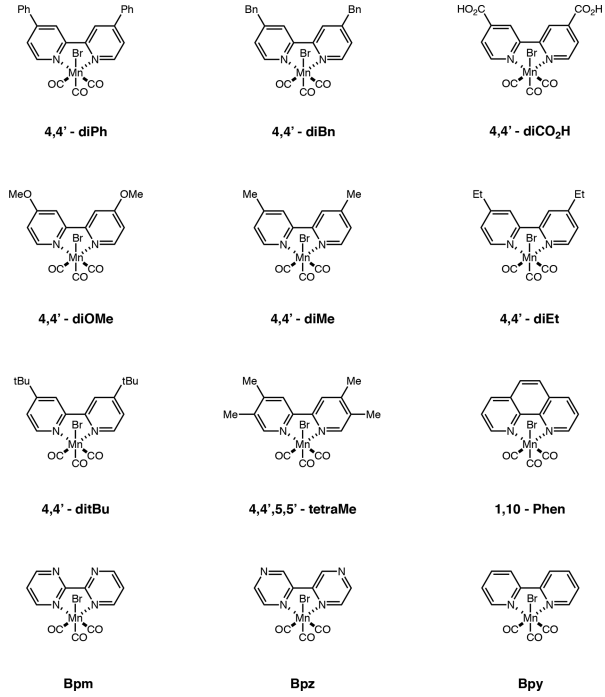

Figure 2. Scope of manganese complexes used in this study.

RESULTS AND DISCUSSION

Complexes were synthesized in one step from manganese pentacarbonyl bromide and the requisite bipyridine ligand. The desired complex was filtered, washed, and characterized. Figure 2 shows the scope of the manganese complexes that were synthesized for the study.

Ultraviolet−visible (UV−vis) spectra were taken for each complex to determine the energy of the metal to ligand charge transfer band (MLCT), a measure of the relative position of the bpy π^* orbital. Cyclic voltammograms with scan rate dependence were then performed to determine the first and second reduction potentials of the complexes. They showed two characteristic reduction waves and a characteristic oxidation wave. The two reduction waves have been attributed as an initial single-electron reduction to arrive at the neutral, pentacoordinate Mn species and a subsequent single-electron reduction to arrive at the anionic Mn species which has been suggested to be the active catalytic intermediate. The reoxidation wave which typically occurs at approximately −0.3 V (vs Ag/Ag^+) has been suggested to be oxidation of a dimeric manganese species. Nicholson and Shain diagnostic tests revealed that the dimer oxidation associated with these catalysts followed an EC mechanism, consistent with a one-electron oxidation of the dimer followed by cleavage of the Mn−Mn bond. Furthermore, the first and second reduction

DOI: 10.1021/acs.organomet.8b00554
Organometallics 2019, 38, 1292−1299

waves exhibited irreversibility in most cases, suggesting slow charge transfer kinetics in comparison to a subsequent chemical step (see the Supporting Information for details).

Density functional theory calculations (DFT) were performed to estimate the highest occupied molecular orbital (HOMO) and lowest unoccupied molecular orbital (LUMO) energy levels and to correlate these energy levels to the MLCT energies as well as first reduction peak potentials from cyclic voltammetry. Table 1 shows the MLCT maxima wavelengths, reduction peak potentials, and calculated LUMO levels for each of the tested complexes.

Table 1. MLCT Transition Wavelengths, LUMO Levels, and First Peak Potentials for the Manganese Complexes Studied[a]

complex	MLCT max (nm)	LUMO (kcal/mol)	first peak potential (V)
4,4′,5,5′-tetraMe	405	−51.5	−1.76
4,4′-diOMe	404	−55.2	−1.65
4,4′-ditBu	412	−55.4	−1.73
4,4′-diEt	412	−55.6	−1.74
4,4′-diMe	412	−56.4	−1.67
1,10-Phen	413	−57.5	−1.51
Bpy	416	−60.4	−1.66
4,4′-diBn	417	−58.8	−1.74
4,4′-diPh	427	−58.8	−1.53
Bpm	430	−80.7	−1.22
4,4′-diCO_2H	459	−79.6	−1.40
Bpz	470	−74.7	−1.23

[a]Peak potentials are reported vs a Ag/Ag^+ (ACN) reference.

As shown from the UV−vis data in Table 1, there is clearly an effect on the bpy π^* level as a result of the varying substitution on the bpy ligand. In comparison to the parent complex, when aryl substituents are placed on the bpy such as a 4,4′-diPh complex, the effect is to red-shift the MLCT, as expected due to the extension of the π system which lowers the π^* energy level. In contrast, the 4,4′-diCO_2H complex, which is electron deficient due to the electron-withdrawing nature of the carboxylic acid substituents, displays a significantly red shifted MLCT absorption level, from 416 nm for the parent manganese complex to 459 nm. Complexes with aliphatic substituents on the bpy such as diMe, diEt, and di*t*Bu display MLCT energies similar to that of the parent manganese complex. The MLCT energy of the 4,4′-diOMe complex is slightly blue shifted (404 nm) in comparison to the parent complex or the aliphatic substituted bpy complexes.

The first peak potentials from cyclic voltammetry as well as the calculation data also reflect these variable bpy π^* energies. The data show that there are no significant differences between the aliphatic substituents or the electron-donating methoxy substituents, as seen in the UV−vis spectra. Additionally, the first reduction peak potential and LUMO level for the 4,4′-diCO_2H-substituted bipyridine is dramatically red shifted and further demonstrates the propensity of this substituent to withdraw electron density from the bpy. These trends are highlighted in Figure 3, in which the relationship between MLCT wavelength vs LUMO level is shown (Figure 3a) as well as the relationship between the first reduction peak potential vs LUMO level (Figure 3b). In both cases there is a clear linear relationship between the two variables, supported by the R^2 values. Furthermore, we observed a strong correlation of the MLCT wavelength and the para-substituted Hammett parameter (Figure 3c) as well as the calculated LUMO energy and the para-substituted Hammett parameter (Figure 3d).[38]

Bulk electrolyses for each of the complexes were then performed to gain insight into how the electronics summarized above affect the efficiency and rate of CO_2 reduction (Table 2). Notably, the remaining efficiency for each complex was accounted for by hydrogen production; there was no detected formate for the electrolyses. Complexes with aliphatic substituents behaved similarly and did not have dramatically different efficiencies of CO_2 reduction. There was a trend within these catalysts toward higher efficiencies when the 4,4′-substituents became increasingly bulkier. This is in agreement with Kubiak's work suggesting that increasing the steric bulk at the 4,4′-position of the bipyridine precludes the off-cycle dimerization step and increases catalytic efficiency.[29] We acknowledge that there have been reports which emphasize that the formation of a Mn−Mn metal bonded dimeric intermediate is the catalytically important species undergoing CO_2 addition and reduction.[39] Our data, however, are in agreement with the conclusions of Kubiak's work and indicate that increasing steric bulk increases the efficiency of the catalysis, presumably due to the bulky substituents impeding the dimerization pathway. Interestingly, complexes with significant electron deficiency as evidenced by their red-shifted MLCT bands, anodically shifted first reduction peak potentials, and lower calculated LUMO levels were almost completely catalytically inactive for CO_2 reduction. Complexes which typified this category were the 4,4′-diCO_2H, Mn-bpz, and Mn-bpm species, which have low currents, indicating slow charge transfer kinetics, and were nearly completely ineffective for CO_2 reduction. There did not seem to be any significant advantage to appending electron-donating substituents, as the 4,4′-diOMe complex was similar to the parent complex's aliphatic derivatives.

In addition to determining the Faradaic efficiencies and the CO production rates, we elected to use the catalytic power efficiency parameter we recently introduced as a measure of how active each catalyst is toward the reduction of CO_2.[40] This parameter incorporates the Faradaic efficiency, the rate of product formation, and the overpotential needed to conduct the reaction as a single mechanism-independent measure of electrocatalytic efficiency. When all three of these parameters are accounted for, an overall measure of catalytic ability is represented and therefore catalysts which have different efficiencies, rates, and overpotentials for product formation may be compared through the use of one dimensionless parameter.

The catalytic power efficiency parameter was calculated according to a previous report and contained information relating to each catalyst's Faradaic efficiency for CO production, its CO production rate, and its overpotential for CO formation. These data are contained in the equation

$$\xi_{cat.} = \frac{j_{obs}}{j_{largest}} \frac{E'_{obs}}{E_{applied}}$$

Here, the current term (numerator and denominator) is the average partial current for the particular catalyst (Q_{tot}/time) divided by the average partial current for the substrate which displayed the largest average partial current density. This

DOI: 10.1021/acs.organomet.8b00554
Organometallics 2019, 38, 1292−1299

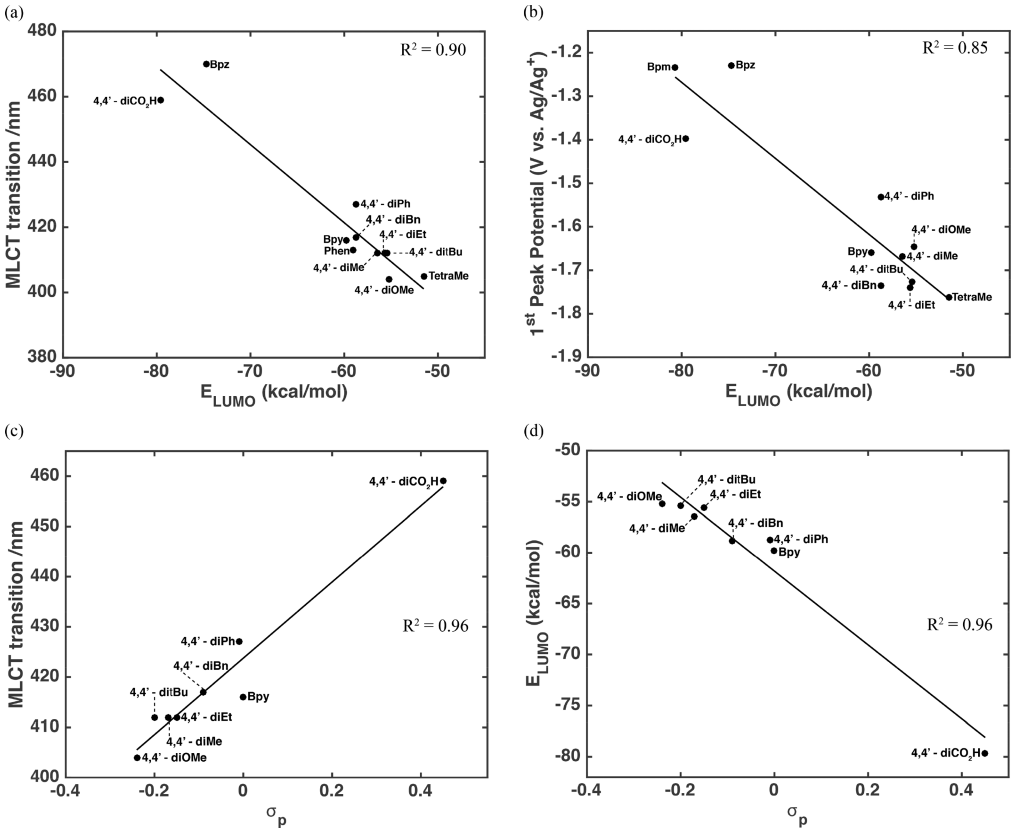

Figure 3. (a) MLCT transition wavelength vs calculated LUMO energy. (b) First reduction peak potential vs calculated LUMO level. (c) MLCT transition wavelength vs para-substituted Hammett parameter (σ_p). (d) Calculated LUMO energy vs σ_p.

Table 2. Faradaic Efficiencies, CO Formation Rates, and Catalytic Efficiency Parameters for Each of the Complexes Tested[a]

complex	FE_{CO} (%)	CO production rate (μmol/min)	catalytic efficiency
4,4′,5,5′-tetraMe	35.8	0.19	0.20
4,4′-diOMe	34.5	0.38	0.45
4,4′-ditBu	23.9	0.24	0.27
4,4′-diEt	49.6	0.51	0.59
4,4′-diMe	25.0	0.29	0.38
1,10 - Phen	17.8	0.17	0.16
4,4′-diBn	50.0	0.18	0.22
4,4′-diPh	14.0	0.06	0.09
4,4′-diCO$_2$H	19.4	0.04	0.05

[a]The Bpm and Bpz complexes are omitted from this table because they did not produce any CO.

normalizes the series of complexes, making the term unity for the species which has the largest average partial current density for CO production. This term therefore accounts for the Faradaic efficiency and the rate of CO production. Thus, the potential term accounts for the overpotential. Here, the numerator term (E'_{obs}) is equal to the negative of the overpotential (assuming the overpotential is a positive value) referenced to an arbitrarily negative potential (2.5 V chosen here). The denominator is equal to the redox potential (assuming the redox potential is a negative value for CO_2 to CO conversion) referenced to the same arbitrary negative potential as the numerator. Thus, if a complex had zero overpotential and also had the largest partial current density for CO in the series of complexes tested, its catalytic power efficiency would be 1; the further a catalyst deviates from ideal parameters (i.e., larger overpotential, slower CO production rate, or lower efficiency), the more its catalytic power efficiency tends toward 0.

As further evidence, we became interested in using the 4,4′-diCO$_2$H complex to demonstrate that shifting the energetics of the π^* orbital affects catalysis. Specifically, we envisioned a simple deprotonation of this complex would blue shift its MLCT, as the carboxylic acid functionality is far more electron withdrawing than the corresponding carboxylate. This idea was realized by showing the blue shifting of the MLCT by 42 nm (6.27 kcal/mol difference) under basic in comparison to acidic conditions (Figure 4a) and a corresponding 3-fold increase in CO production rate under the basic vs acidic conditions (Figure 4b). Under the same conditions for the parent complex there was no measurable difference in the CO production rate. These data exemplify how modulation of the bpy π^* level dramatically affects the resulting CO_2 reduction capabilities of these catalysts.

With these data in hand, we hypothesize the qualitative molecular orbital picture shown in Figure 5 to rationalize our observations. In this scheme, a nondegenerate, filled set of metal d−π orbitals is energetically lower than an empty bpy π^* and two metal d−σ^* orbitals. An initial reduction step puts one electron in the bpy π^* orbital, which we suggest must undergo a charge transfer to the metal d−σ^* orbital corresponding to the Mn−Br bond to induce loss of the axial bromide and generate the active Mn catalyst for CO_2 reduction. A similar mechanism was suggestd by Vlček for the electrochemically induced loss of CO from [Cr(bpy)(CO)$_4$].[41] In the case of nonbiasing substituents or electron-donating substituents,

DOI: 10.1021/acs.organomet.8b00554
Organometallics 2019, 38, 1292−1299

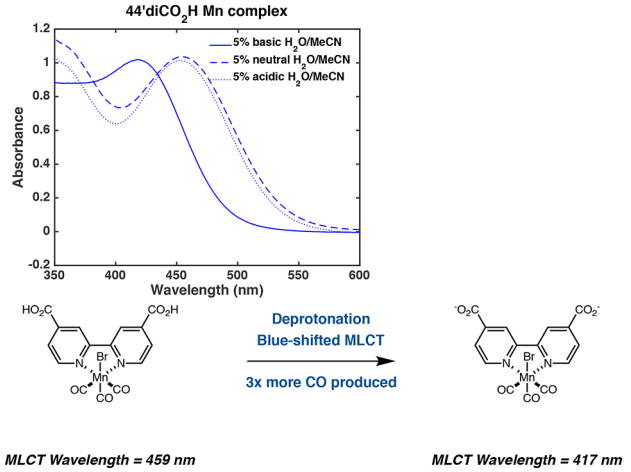

Figure 4. UV−vis spectra of 4,4′-diCO_2H under protonated and unprotonated conditions. Results from bulk electrolysis show that the carboxylate complex catalyzed CO_2 reduction ∼3× faster in comparison to the protonated complex.

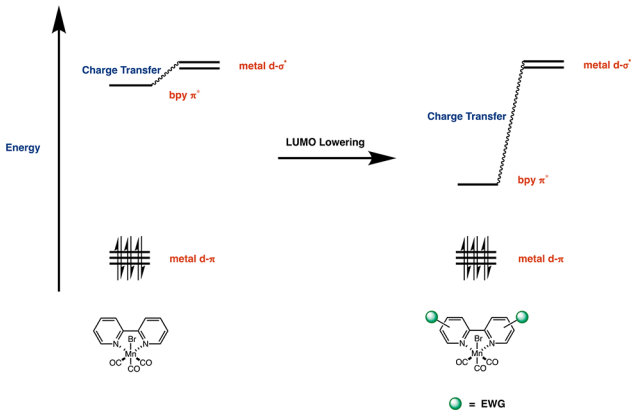

Figure 5. Schematic diagram of the effect of appending electron-withdrawing groups to the bipyridine as it relates to lowering the bpy π^* level. EWG = electron-withdrawing group.

facile charge transfer from the bpy π^* to the Mn−Br σ^* should be possible due to the similar energies of these two orbitals. However, when electron-withdrawing substituents are placed on the bipyridine, they lower the bpy π^* level, increasing the energy difference between the bpy π^* and the Mn−Br σ^* levels, thereby decreasing the feasibility of the charge transfer. This model is supported by DFT calculations which show that, in comparison to the parent complex, the gap between the bpy π^* and the Mn−Br σ^* for the 4,4′-diCO_2H complex is greater than 10 kcal/mol.

Related to the LUMO energy level modifications affecting the charge transfer to the Mn−Br σ^* are the energy level modifications to the HOMO energy level of the doubly reduced complex. The HOMO of the doubly reduced complex is responsible for effective binding to a molecule of CO_2. Therefore, attaching substituents that withdraw electron density from the metal center, and thus the HOMO for binding CO_2, would be expected to reduce the catalyst's ability to bind CO_2 and catalyze CO_2 reduction. The variability in the HOMO energy level of the doubly reduced state was examined through DFT calculations (Supporting Information). The HOMO levels for the electron-deficient complexes, such as the 4,4′-diCO_2H complex or the Bpz complex, are significantly more negative than the electron-neutral or electron-rich complexes. We suggest that this difference is likely to have an effect on the rate of catalysis of these complexes, as the HOMO of the doubly reduced complex is responsible for binding a molecule of CO_2.

A note about the 1,10-Phen complex is necessary. This complex displays UV−vis, CV, and calculation data similar to those of the parent bipyridine-manganese complex. It would therefore be expected to behave similarly in an electrolysis experiment when held at the same potential. However, this species is significantly less effective at transforming CO_2 into CO. This may be a result of the inability of the 1,10-phenanthroline ligand to rotate about the biaryl bond. Rotation about this bond is likely to provide better overlap between the bpy π^* and the Mn−Br σ^* orbitals, facilitating the requisite internal charge transfer. Thus, inhibiting this rotation could account for the disparity between the 1,10-Phen complex and the traditional bipyridine-based catalysts.

CONCLUSION

A series of electronically and sterically differentiated manganese complexes were synthesized. Their electronic properties were studied using UV−vis spectrophotometry, cyclic voltammetry, and DFT calculations. The catalytic ability to reduce CO_2 was then studied using a series of electrolysis experiments, and the efficiencies and rates of CO production were compared to the electronic property measurements taken previously. Electronically deficient species were not able to act as catalysts for the conversion of CO_2 to CO, while species with unbiasing or electron-donating substituents on the bipyridine were effective catalysts for CO_2 reduction, with catalytic efficiency generally increasing as the steric bulk of the substituents increased. The inability of CO_2 reduction using electron-deficient complexes is hypothesized to be due to the combination of two factors. First, loss of the axial bromide is slower for electron-deficient complexes due to the difficulty of the internal charge transfer step. Second, less electron density in the HOMO of the doubly reduced state of electron-deficient complexes makes it more difficult to bind a molecule of CO_2. These are supported by a series of DFT calculations showing and the lowering of the LUMO level for the bromide-precursor complexes as well as the HOMO energy level on the doubly reduced complex is significantly higher for electron-neutral or -rich complexes in comparison to the electron deficient complexes. Further studies will be performed to explain the relatively poor efficiency of the Phen complex to reduce CO_2, given all of its similarities to species which reduce CO_2 more effectively.

EXPERIMENTAL SECTION

General Procedure. Synthetic reactions were conducted using standard Schlenk-line techniques under an atmosphere of argon. For all electrochemical experiments, the electrolyte was bubbled with the desired gas (argon or CO_2) for 15 min prior to taking a background scan to ensure a featureless background from 0 to −2.8 vs Ag/Ag^+. After the desired complex was added, the electrolyte was bubbled for an additional 5 min prior to data collection. Complexes were loaded at a concentration of 1 mM for both CV and bulk electrolysis. Ferrocene was added as an internal reference. The total colume of electrolyte used for these experiments was 10 mL for CV and 25 mL for bulk electrolysis. Bulk electrolyses were operated for ∼4 h, and the headspace was analyzed by GC approximately every 20 min. The proton concentration was kept consisten for argon and CO_2 trials by

DOI: 10.1021/acs.organomet.8b00554
Organometallics 2019, 38, 1292−1299

using pH-adjusted water with $HClO_4$ in the case of argon and neutral water in the case of CO_2.

Materials. All reagents (reagent grade) were obtained from commercial suppliers and used without further purification unless otherwise noted. Anhydrous acetonitrile (MeCN) and dichloromethane (CH_2Cl_2) were purchased from Sigma-Aldrich (Sure/Seal). Tetrabutylammonium hexafluorophosphate ($TBAPF_6$, Sigma-Aldrich) was dried under vacuum overnight prior to use. Manganese pentacarbonyl bromide (Strem), 2,2′-bipyridine (bpy, Sigma-Aldrich), 2,2′-bipyrimidine (bpm, TGI), 2,2′-bipyrazine (bpz, Sigma-Aldrich), and 1,10-phenanthroline (phen, Sigma-Aldrich) were used as received. Manganese complexes were carefully handled with minimal light exposure. [Mn(bpy)$(CO)_3$Br], [Mn(phen)$(CO)_3$Br], [Mn(bpm)$(CO)_3$Br], [Mn(4,4′-diCO_2H)$(CO)_3$Br], [Mn(4,4′-diMe)$(CO)_3$Br], and [Mn(4,4′-ditBu)$(CO)_3$Br] were synthesized according to published methods.[18,28,42−45] Electrolytes were prepared by dissolving $TBAPF_6$ in anhydrous MeCN or DMF (for the study of Mn(bpz)$(CO)_3$Br) in a Schlenk flask. The electrolyte was stored under an inert atmosphere and purged immediately prior to use. A 3 mm glassy-carbon-disk electrode (BASi MF-2012) was used in all electrochemical experiments. Potentials are referenced to an Ag/$AgNO_3$ (10 mM) electrode (BASi MW-1085) in 0.1 M TBAP/MeCN. A silver-wire pseudoreference electrode was used in 0.1 M TBAP/DMF, and the potential was further converted to Ag/Ag^+ by ferrocene/ferrocenium internal standard. A platinum mesh (~1 cm^2) attached to a platinum wire was used as the counter electrode in all electrochemical measurements. A 15 mL three-neck round-bottom flask was used as the electrochemical cell for CV, and a 70 mL four-neck homemade jacketed flask was used for bulk electrolysis. The working electrode and reference electrodes were secured using "mini" Ace-threaded adaptors from Ace glass (No. 7 and No. 8, respectively). The counter electrode was threaded through a septum, which was then fitted onto one neck of the cell.

Instrumentation. Electrochemical measurements were performed on a Model CHI 760D electrochemical workstation (CH Instruments, Austin, TX). Nuclear magnetic resonance (NMR) spectra were recorded on a Bruker AVANCE spectrometer (500 MHz for ^1H nuclei and 125 MHz for ^{13}C nuclei). Chemical shifts are reported in parts per million (ppm) downfield of tetramethylsilane and are referenced to the solvent residual peak. Infrared spectra for solid samples were recorded on a Nicolet Model 6700 FT-IR spectrometer equipped with a single-reflection diamond ATR attachment. UV−vis spectra were monitored using a Cary 60 UV−vis spectrophotometer (Agilent Technologies). CO production was analyzed using a 60 °C isothermal method over 5 min on a HP 6890 gas chromatograph and TCD with a Molsieve 5A PLOT capillary column (Agilent) and He as the flow gas. H_2 was sampled with an SRI 8610C gas chromatograph and TCD with a Molsieve column (HAYESEP D) and Ar flow gas. A 7 min isotherm at 80 °C was employed.

Computational Methodology. Geometry optimization and frequency calculations of the ground-state, one-electron-reduced, and two-electron-reduced complexes were performed using Gaussian 16 on density functional theory (DFT) with the M06 functional level of theory and 6-311G** basis set. In addition, a LANL2DZ basis set was applied on the manganese metal center to describe inner electrons with effective core potentials. Excited state (S_1 and T_1) geometry and frequency calculations were carried out using time-dependent DFT (TD-DFT) on the gas-phase optimized ground-state geometry with B3LYP functional level. All frequency calculations carried out on stationary points yielded zero imaginary frequencies. HOMO and LUMO energy levels were extracted from the calculations.

Preparation of Mn(bpz)$(CO)_3$Br. A slurry of $Mn(CO)_5Br$ (0.16 g, 0.58 mmol) and 2,2′-bipyrazine (0.09 g, 0.57 mmol) in MeOH (15 mL) was refluxed at 65 °C for 3 h in the dark. After it was cooled to 0 °C, the mixture was filtered and washed with chilled MeOH. After reprecipitation from CH_2Cl_2/diethyl ether a dark red powder was obtained to afford 0.16 g (75% yield). UV−vis data in MeCN (λ_{max}, nm): 470. IR (ATR-IR, cm^{-1}): 2036 (s), 1927 (w). ^1H NMR (500 MHz, DMSO-d_6): δ 10.01 (s, 2H), 9.36 (d, 2H), 8.92 (d, 2H). $^{13}C\{^1H\}$ NMR (126 MHz, DMSO-d_6): δ 222.22, 218.59, 148.99, 147.89, 146.90, 144.55.

Preparation of Mn(4,4′-diPh)$(CO)_3$Br. A mixture of Mn$(CO)_5$Br (0.20 g, 0.73 mmol) and 4,4′-diphenyl-2,2′-bipyridine (0.234 g, 0.76 mmol) in diethyl ether (40 mL) was refluxed for 3 h in the dark. The reaction mixture was filtered, and the filtrate, which was washed several times with cold diethyl ether, was dried in vacuo to afford 0.21 g (54% yield). UV−vis data in MeCN (λ_{max}, nm): 427. IR (ATR-IR, cm^{-1}): 2022 (m), 1925 (m), 1892 (s). ^1H NMR (500 MHz, DMSO-d_6): δ 9.19 (d, 4H), 8.09 (m, 6H), 7.64 (m, 6H) . $^{13}C\{^1H\}$ NMR (126 MHz, DMSO-d_6): δ 156.33, 154.12, 150.60, 135.95, 130.95, 129.79, 128.09, 124.50, 121.38.

Preparation of Mn(4,4′-diBn)$(CO)_3$Br. A mixture of Mn$(CO)_5$Br (0.20 g, 0.73 mmol) and 4,4′-dibenzyl-2,2′-bipyridine (0.255 g, 0.76 mmol) in diethyl ether (40 mL) was refluxed for 3 h in the dark. The reaction mixture was filtered, and the filtrate, which was washed several times with cold diethyl ether, was dried in vacuo to afford 0.25 g (62% yield). UV−vis data in MeCN (λ_{max}, nm): 417. IR (ATR-IR, cm^{-1}): 2018 (s), 1905 (s). ^1H NMR (500 MHz, DMSO-d_6): δ 9.04 (d, 2H), 8.61 (s, 2H), 7.53 (d, 2H), 7.37 (m, 10H), 4.18 (s, 4H). $^{13}C\{^1H\}$ NMR (126 MHz, DMSO-d_6): δ 155.53, 154.43, 153.80, 139.12, 129.39, 129.31, 129.13, 127.41, 127.26, 123.86.

Preparation of Mn(4,4′-diOMe)$(CO)_3$Br. A mixture of Mn$(CO)_5$Br (0.20 g, 0.73 mmol) and 4,4′-dimethoxy-2,2′-bipyridine (0.164 g, 0.76 mmol) in diethyl ether (40 mL) was refluxed for 3 h in the dark. The reaction mixture was filtered, and the filtrate, which was washed several times with cold diethyl ether, was dried in vacuo to afford 0.23 g (73% yield). UV−vis data in MeCN (λ_{max}, nm): 404. IR (ATR-IR, cm^{-1}): 2023 (m), 1900 (s). ^1H NMR (500 MHz, DMSO-d_6): δ 8.92 (d, 2H), 8.26 (s, 2H), 7.31 (d, 2H), 4.04 (s, 6H). $^{13}C\{^1H\}$ NMR (126 MHz, DMSO-d_6): δ 168.12, 157.09, 154.58, 110.37, 57.08.

Preparation of Mn(4,4′-diEt)$(CO)_3$Br. A mixture of $Mn(CO)_5Br$ (0.20 g, 0.73 mmol) and 4,4′-diethyl-2,2′-bipyridine (0.161 g, 0.76 mmol) in diethyl ether (40 mL) was refluxed for 3 h in the dark. The reaction mixture was filtered, and the filtrate, which was washed several times with cold diethyl ether, was dried in vacuo to afford 0.22 g (71% yield). UV−vis data in MeCN (λ_{max}, nm): 412. IR (ATR-IR, cm^{-1}): 2015 (s), 1901 (s). ^1H NMR (500 MHz, DMSO-d_6): δ 9.02 (d, 2H), 8.57 (s, 2H), 7.59 (d, 2H), 2.84 (q, 4H), 1.31 (t, 6H). $^{13}C\{^1H\}$ NMR (126 MHz, DMSO-d_6): δ 156.85, 155.36, 153.41, 126.57, 123.20, 28.05, 14.59.

Preparation of Mn(4,4′,5,5′-tetraMe)$(CO)_3$Br. A mixture of $Mn(CO)_5Br$ (0.20 g, 0.73 mmol) and 4,4′,5,5′-tetramethyl-2,2′-bipyridine (0.161 g, 0.76 mmol) in diethyl ether (40 mL) was refluxed for 3 h in the dark. The reaction mixture was filtered, and the filtrate, which was washed several times with cold diethyl ether, was dried in vacuo to afford 0.21 g (66% yield). UV−vis data in MeCN (λ_{max}, nm): 405. IR (ATR-IR, cm^{-1}): 2018 (s), 1898 (s), 1931 (sh). ^1H NMR (500 MHz, DMSO-d_6): δ 8.83 (s, 2H), 8.41 (s, 2H), 2.45 (s, 6H), 2.38 (s, 6H). $^{13}C\{^1H\}$ NMR (126 MHz, DMSO-d_6): δ 152.39, 150.20, 136.19, 123.67, 19.44, 16.54.

■ ASSOCIATED CONTENT

Supporting Information

The Supporting Information is available free of charge on the ACS Publications website at DOI: 10.1021/acs.organomet.8b00554.

Cyclic voltammograms, UV−vis spectra, HOMO levels of the doubly reduced complexes, and coordinates for geometry-optimized structures (PDF)

Cartesian coordinates for the calculated structures (ZIP)

■ AUTHOR INFORMATION

Corresponding Author

*E-mailfor A.B.B.: bocarsly@princeton.edu.

DOI: 10.1021/acs.organomet.8b00554
Organometallics 2019, 38, 1292−1299

ORCID

Hsin-Ya Kuo: 0000-0003-0194-3716
Tia S. Lee: 0000-0003-0635-6668
Gregory D. Scholes: 0000-0003-3336-7960
Andrew B. Bocarsly: 0000-0003-3718-0933

Notes

The authors declare no competing financial interest.

■ ACKNOWLEDGMENTS

Financial support for this work was provided by the National Science Foundation under grant CHE-1800400. G.D.S. acknowledges support from the Division of Chemical Sciences, Geosciences, and Biosciences, Office of Basic Energy Sciences of the U.S. Department of Energy, through Grant No. DE-SC0015429. Any opinions, findings, and conclusions or recommendations expressed in this material are those of the authors and do not necessarily reflect the views of the National Science Foundation.

■ REFERENCES

(1) Song, C. Global Challenges and Strategies for Control, Conversion and Utilization of CO_2 for Sustainable Development Involving Energy, Catalysis, Adsorption and Chemical Processing. *Catal. Today* **2006**, *115* (1), 2−32.

(2) Rohling, E. J.; Rohling, E. J.; Sluijs, A.; Dijkstra, H. A.; Köhler, P.; Wal, R. S. W.; Heydt, A. S.; Beerling, D. J.; Berger, A.; et al. Making Sense of Palaeoclimate Sensitivity. *Nature* **2012**, *491* (7426), 683−691.

(3) Leitner, W. Carbon Dioxide as a Raw Material: The Synthesis of Formic Acid and Its Derivatives from CO_2. *Angew. Chem., Int. Ed. Engl.* **1995**, *34* (20), 2207−2221.

(4) Schreier, M.; Héroguel, F.; Steier, L.; Ahmad, S.; Luterbacher, J. S.; Mayer, M. T.; Luo, J.; Grätzel, M. Solar Conversion of CO_2 to CO Using Earth-Abundant Electrocatalysts Prepared by Atomic Layer Modification of CuO. *Nat. Energy* **2017**, *2* (7), 17087.

(5) Gattrell, M.; Gupta, N.; Co, A. A Review of the Aqueous Electrochemical Reduction of CO_2 to Hydrocarbons at Copper. *J. Electroanal. Chem.* **2006**, *594* (1), 1−19.

(6) Chen, Y.; Li, C. W.; Kanan, M. W. Aqueous CO_2 Reduction at Very Low Overpotential on Oxide-Derived Au Nanoparticles. *J. Am. Chem. Soc.* **2012**, *134* (49), 19969−19972.

(7) Hara, K.; Kudo, A.; Sakata, T. Electrochemical Reduction of Carbon Dioxide under High Pressure on Various Electrodes in an Aqueous Electrolyte. *J. Electroanal. Chem.* **1995**, *391* (1), 141−147.

(8) Kimura, K. W.; Fritz, K. E.; Kim, J.; Suntivich, J.; Abruña, H. D.; Hanrath, T. Controlled Selectivity of CO_2 Reduction on Copper by Pulsing the Electrochemical Potential. *ChemSusChem* **2018**, *11* (11), 1781−1786.

(9) Hori, Y.; Wakebe, H.; Tsukamoto, T.; Koga, O. Electrocatalytic Process of CO Selectivity in Electrochemical Reduction of CO_2 at Metal Electrodes in Aqueous Media. *Electrochim. Acta* **1994**, *39* (11), 1833−1839.

(10) Hori, Y. Electrochemical CO_2 Reduction on Metal Electrodes. In *Modern Aspects of Electrochemistry*; Springer, New York, 2008; pp 89−189.

(11) Abruña, H. D. Coordination Chemistry in Two Dimensions: Chemically Modified Electrodes. *Coord. Chem. Rev.* **1988**, *86*, 135−189.

(12) Paris, A. R.; Bocarsly, A. B. Ni−Al Films on Glassy Carbon Electrodes Generate an Array of Oxygenated Organics from CO_2. *ACS Catal.* **2017**, *7* (10), 6815−6820.

(13) Paris, A. R.; Chu, A. T.; O'Brien, C. B.; Frick, J. J.; Francis, S. A.; Bocarsly, A. B. Tuning the Products of CO_2 Electroreduction on a Ni_3Ga Catalyst Using Carbon Solid Supports. *J. Electrochem. Soc.* **2018**, *165* (7), H385−H392.

(14) Torelli, D. A.; Francis, S. A.; Crompton, J. C.; Javier, A.; Thompson, J. R.; Brunschwig, B. S.; Soriaga, M. P.; Lewis, N. S. Nickel−Gallium-Catalyzed Electrochemical Reduction of CO_2 to Highly Reduced Products at Low Overpotentials. *ACS Catal.* **2016**, *6* (3), 2100−2104.

(15) Mulzer, C. R.; Shen, L.; Bisbey, R. P.; McKone, J. R.; Zhang, N.; Abruña, H. D.; Dichtel, W. R. Superior Charge Storage and Power Density of a Conducting Polymer-Modified Covalent Organic Framework. *ACS Cent. Sci.* **2016**, *2* (9), 667−673.

(16) Costentin, C.; Drouet, S.; Robert, M.; Savéant, J.-M. A Local Proton Source Enhances CO_2 Electroreduction to CO by a Molecular Fe Catalyst. *Science* **2012**, *338* (6103), 90−94.

(17) Froehlich, J. D.; Kubiak, C. P. Homogeneous CO_2 Reduction by Ni(Cyclam) at a Glassy Carbon Electrode. *Inorg. Chem.* **2012**, *51* (7), 3932−3934.

(18) Bourrez, M.; Molton, F.; Chardon-Noblat, S.; Deronzier, A. $[Mn(Bipyridyl)(CO)_3Br]$: An Abundant Metal Carbonyl Complex as Efficient Electrocatalyst for CO_2 Reduction. *Angew. Chem., Int. Ed.* **2011**, *50* (42), 9903−9906.

(19) Smieja, J. M.; Kubiak, C. P. $Re(Bipy\text{-}TBu)(CO)_3Cl$−improved Catalytic Activity for Reduction of Carbon Dioxide: IR-Spectroelectrochemical and Mechanistic Studies. *Inorg. Chem.* **2010**, *49* (20), 9283−9289.

(20) Meshitsuka, S.; Ichikawa, M.; Tamaru, K. Electrocatalysis by Metal Phthalocyanines in the Reduction of Carbon Dioxide. *J. Chem. Soc., Chem. Commun.* **1974**, *0* (5), 158−159.

(21) Fisher, B. J.; Eisenberg, R. Electrocatalytic Reduction of Carbon Dioxide by Using Macrocycles of Nickel and Cobalt. *J. Am. Chem. Soc.* **1980**, *102* (24), 7361−7363.

(22) Hawecker, J.; Lehn, J.-M.; Ziessel, R. Electrocatalytic Reduction of Carbon Dioxide Mediated by $Re(Bipy)(CO)_3Cl$ (Bipy = 2,2′-Bipyridine). *J. Chem. Soc., Chem. Commun.* **1984**, *0* (6), 328−330.

(23) Hernández, S.; Farkhondehfal, M. A.; Sastre, F.; Makkee, M.; Saracco, G.; Russo, N. Syngas Production from Electrochemical Reduction of CO_2: Current Status and Prospective Implementation. *Green Chem.* **2017**, *19* (10), 2326−2346.

(24) Agarwal, J.; Stanton, C. J.; Shaw, T. W.; Vandezande, J. E.; Majetich, G. F.; Bocarsly, A. B.; Schaefer, H. F. Exploring the Effect of Axial Ligand Substitution (X = Br, NCS, CN) on the Photodecomposition and Electrochemical Activity of $[MnX(N{-}C)(CO)_3]$ Complexes. *Dalton Trans* **2015**, *44* (5), 2122−2131.

(25) Machan, C. W.; Stanton, C. J.; Vandezande, J. E.; Majetich, G. F.; Schaefer, H. F.; Kubiak, C. P.; Agarwal, J. Electrocatalytic Reduction of Carbon Dioxide by $Mn(CN)(2,2'\text{-Bipyridine})(CO)_3$: CN Coordination Alters Mechanism. *Inorg. Chem.* **2015**, *54* (17), 8849−8856.

(26) Francke, R.; Schille, B.; Roemelt, M. Homogeneously Catalyzed Electroreduction of Carbon Dioxide—Methods, Mechanisms, and Catalysts. *Chem. Rev.* **2018**, *118* (9), 4631−4701.

(27) Sinopoli, A.; La Porte, N. T.; Martinez, J. F.; Wasielewski, M. R.; Sohail, M. Manganese Carbonyl Complexes for CO_2 Reduction. *Coord. Chem. Rev.* **2018**, *365*, 60−74.

(28) Smieja, J. M.; Sampson, M. D.; Grice, K. A.; Benson, E. E.; Froehlich, J. D.; Kubiak, C. P. Manganese as a Substitute for Rhenium in CO_2 Reduction Catalysts: The Importance of Acids. *Inorg. Chem.* **2013**, *52* (5), 2484−2491.

(29) Sampson, M. D.; Nguyen, A. D.; Grice, K. A.; Moore, C. E.; Rheingold, A. L.; Kubiak, C. P. Manganese Catalysts with Bulky Bipyridine Ligands for the Electrocatalytic Reduction of Carbon Dioxide: Eliminating Dimerization and Altering Catalysis. *J. Am. Chem. Soc.* **2014**, *136* (14), 5460−5471.

(30) Agarwal, J.; Shaw, T. W.; Schaefer, H. F.; Bocarsly, A. B. Design of a Catalytic Active Site for Electrochemical CO_2 Reduction with Mn(I)-Tricarbonyl Species. *Inorg. Chem.* **2015**, *54* (11), 5285−5294.

(31) Franco, F.; Cometto, C.; Nencini, L.; Barolo, C.; Sordello, F.; Minero, C.; Fiedler, J.; Robert, M.; Gobetto, R.; Nervi, C. Local Proton Source in Electrocatalytic CO_2 Reduction with $[Mn(Bpy{-}R)(CO)_3Br]$ Complexes. *Chem. - Eur. J.* **2017**, *23* (20), 4782−4793.

DOI: 10.1021/acs.organomet.8b00554
Organometallics 2019, 38, 1292−1299

(32) Clark, M. L.; Cheung, P. L.; Lessio, M.; Carter, E. A.; Kubiak, C. P. Kinetic and Mechanistic Effects of Bipyridine (Bpy) Substituent, Labile Ligand, and Brønsted Acid on Electrocatalytic CO_2 Reduction by Re(Bpy) Complexes. *ACS Catal.* **2018**, *8* (3), 2021−2029.
(33) Riplinger, C.; Sampson, M. D.; Ritzmann, A. M.; Kubiak, C. P.; Carter, E. A. Mechanistic Contrasts between Manganese and Rhenium Bipyridine Electrocatalysts for the Reduction of Carbon Dioxide. *J. Am. Chem. Soc.* **2014**, *136* (46), 16285−16298.
(34) Stanton, C. J.; Vandezande, J. E.; Majetich, G. F.; Schaefer, H. F.; Agarwal, J. Mn-NHC Electrocatalysts: Increasing π Acidity Lowers the Reduction Potential and Increases the Turnover Frequency for CO_2 Reduction. *Inorg. Chem.* **2016**, *55* (19), 9509−9512.
(35) Agarwal, J.; Shaw, T. W.; Stanton, C. J.; Majetich, G. F.; Bocarsly, A. B.; Schaefer, H. F. NHC-Containing Manganese(I) Electrocatalysts for the Two-Electron Reduction of CO_2. *Angew. Chem., Int. Ed.* **2014**, *53* (20), 5152−5155.
(36) Grice, K. A.; Kubiak, C. P.; Aresta, M.; van Eldik, R. Chapter Five - Recent Studies of Rhenium and Manganese Bipyridine Carbonyl Catalysts for the Electrochemical Reduction of CO_2. *Adv. Inorg. Chem.* **2014**, *66*, 163−188.
(37) Ngo, K. T.; McKinnon, M.; Mahanti, B.; Narayanan, R.; Grills, D. C.; Ertem, M. Z.; Rochford, J. Turning on the Protonation-First Pathway for Electrocatalytic CO_2 Reduction by Manganese Bipyridyl Tricarbonyl Complexes. *J. Am. Chem. Soc.* **2017**, *139* (7), 2604−2618.
(38) Hansch, C.; Leo, A.; Taft, R. W. A Survey of Hammett Substituent Constants and Resonance and Field Parameters. *Chem. Rev.* **1991**, *91* (2), 165−195.
(39) Bourrez, M.; Orio, M.; Molton, F.; Vezin, H.; Duboc, C.; Deronzier, A.; Chardon-Noblat, S. Pulsed-EPR Evidence of a Manganese(II) Hydroxycarbonyl Intermediate in the Electrocatalytic Reduction of Carbon Dioxide by a Manganese Bipyridyl Derivative. *Angew. Chem., Int. Ed.* **2014**, *53* (1), 240−243.
(40) Pander, J. E.; Fogg, A.; Bocarsly, A. B. Utilization of Electropolymerized Films of Cobalt Porphyrin for the Reduction of Carbon Dioxide in Aqueous Media. *ChemCatChem* **2016**, *8* (22), 3536−3545.
(41) Farrell, I. R.; Matousek, P.; Towrie, M.; Parker, A. W.; Grills, D. C.; George, M. W.; Vlček, A. Direct Observation of Competitive Ultrafast CO Dissociation and Relaxation of an MLCT Excited State: Picosecond Time-Resolved Infrared Spectroscopic Study of [Cr-$(CO)_4$(2,2′-Bipyridine)]. *Inorg. Chem.* **2002**, *41* (17), 4318−4323.
(42) Walsh, J. J.; Smith, C. L.; Neri, G.; Whitehead, G. F. S.; Robertson, C. M.; Cowan, A. J. Improving the Efficiency of Electrochemical CO_2 Reduction Using Immobilized Manganese Complexes. *Faraday Discuss.* **2015**, *183* (0), 147−160.
(43) Kumar, P.; Joshi, C.; Srivastava, A. K.; Gupta, P.; Boukherroub, R.; Jain, S. L. Visible Light Assisted Photocatalytic [3 + 2] Azide−Alkyne "Click" Reaction for the Synthesis of 1,4-Substituted 1,2,3-Triazoles Using a Novel Bimetallic Ru−Mn Complex. *ACS Sustainable Chem. Eng.* **2016**, *4* (1), 69−75.
(44) Twala, T. N.; Schutte-Smith, M.; Roodt, A.; Visser, H. G. Activation of the Manganese(I) Tricarbonyl Core by Selective Variation of Bidentate Ligands (L,L′-Bid = N,N′ and N,O Donor Atom Sets) in Fac-[Mn$(CO)_3$(L,L′-Bid)(CH3OH)]n Complexes. *Dalton Trans* **2015**, *44* (7), 3278−3288.
(45) Jimenez, J.; Chakraborty, I.; Mascharak, P. K. Synthesis and Assessment of CO-Release Capacity of Manganese Carbonyl Complexes Derived from Rigid α-Diimine Ligands of Varied Complexity. *Eur. J. Inorg. Chem.* **2015**, *2015* (30), 5021−5026.

DOI: 10.1021/acs.organomet.8b00554
Organometallics 2019, 38, 1292−1299